International Journal of Nanomedicine

Dovepress
open access to scientific and medical research

Open Access Full Text Article

ORIGINAL RESEARCH

Bovine Serum Albumin – Hydroxyapatite Nanoflowers as Potential Local Drug Delivery System of Ciprofloxacin

Kornelia Bobrowska[1], Kamila Sadowska[1], Krzysztof Stolarczyk[2], Marta Prześniak-Welenc[3], Piotr Golec[4], Renata Bilewicz[2]

[1]Nalecz Institute of Biocybernetics and Biomedical Engineering, Polish Academy of Sciences, Warsaw, Poland; [2]Faculty of Chemistry, University of Warsaw, Warsaw, Poland; [3]Institute of Nanotechnology and Materials Engineering, and Advanced Materials Centre, Gdansk University of Technology, Gdansk, Poland; [4]Department of Molecular Virology, Institute of Microbiology, Faculty of Biology, University of Warsaw, Warsaw, Poland

Correspondence: Kamila Sadowska, Nalecz Institute of Biocybernetics and Biomedical Engineering, Polish Academy of Sciences, Ks. Trojdena 4, Warsaw, 02-109, Poland, Tel +48 22 59 25 140, Email ksadowska@ibib.waw.pl

Introduction: Hybrid nanoflowers are structures consisting of organic (enzymes, proteins, nucleic acids) and inorganic components (mostly metal phosphates) with a flower-like hierarchical structure. Novel hybrid nanoflowers based on bovine serum albumin (BSA) and hydroxyapatite (HA) were obtained and characterized. Study on BSA-HA nanoflowers as potential drug delivery system is reported for the first time.

Methods: Embedding ciprofloxacin in the structure of hybrid nanoflowers was confirmed by ATR-FTIR and thermogravimetric analysis. The inorganic phase of the nanoflowers was determined by X-ray diffraction. UV–Vis spectroscopy was used to evaluate the release profiles of ciprofloxacin from nanoflowers in buffer solutions at pH 7.4 and 5. The agar disk diffusion method was used to study the antibacterial activity of the synthesized nanoflowers against *Staphylococcus aureus* and *Pseudomonas aeruginosa*.

Results: Bovine serum albumin – hydroxyapatite nanoflowers were obtained with diameters of ca. 1–2 μm. The kinetics of ciprofloxacin release from nanoflowers were described by the Korsmeyer-Peppas model. The antibacterial activity of the synthesized nanoflowers was demonstrated against *S. aureus* and *P. aeruginosa*, two main pathogens found in osteomyelitis.

Conclusion: The formulated nanoflowers may act as an efficient local antibiotic delivery system. Due to the use of nonhazardous, biodegradable components and benign synthesis, hybrid nanoflowers are very promising drug delivery systems that could be applied in the treatment of skeletal system infections.

Keywords: hybrid nanoflowers, organic–inorganic nanoflowers, *Staphylococcus aureus*, *Pseudomonas aeruginosa*, *osteomyelitis*

Introduction

A drug delivery system (DDS) is defined as a formulation or device that allows the introduction of a drug substance into the body and improves the therapeutic effect and safety by controlling the rate, time and location of drug release in the body.[1] Using DDS, drugs may be administered locally to the place affected by disease or given systemically and targeted to the diseased organ.[2] Our group used various nanomaterials and molecules, such as gold nanoparticles,[3–7] cyclodextrins[8–10] and cubic phase nanoparticles – cubosomes[11–14] – as drug carriers for systemic or local administration of chemotherapeutics. In this paper, we present a simple, one-step, room temperature synthesis of organic–inorganic hybrid nanoflowers as a potential DDS of ciprofloxacin for osteomyelitis treatment. Osteomyelitis is an inflammation of the bone tissue and bone marrow, caused mainly by *Staphylococcus aureus* and *Pseudomonas aeruginosa*,[15] which is one of the most difficult infectious diseases to treat. Statistically, it affects 1 in 5000 people under the age of 13 and approximately 2% of all patients after surgical interventions. Currently, the main problem in the treatment of infections is the increasing resistance of bacteria to antimicrobial agents. This is mainly due to improper, too short or excessive use of antibiotics. Unfortunately, the number of bacterial strains showing resistance to antimicrobials and the range of resistance continues to increase. Scientists estimate that by 2050,

Received: 28 July 2023
Accepted: 5 October 2023
Published: 8 November 2023

Graphical Abstract

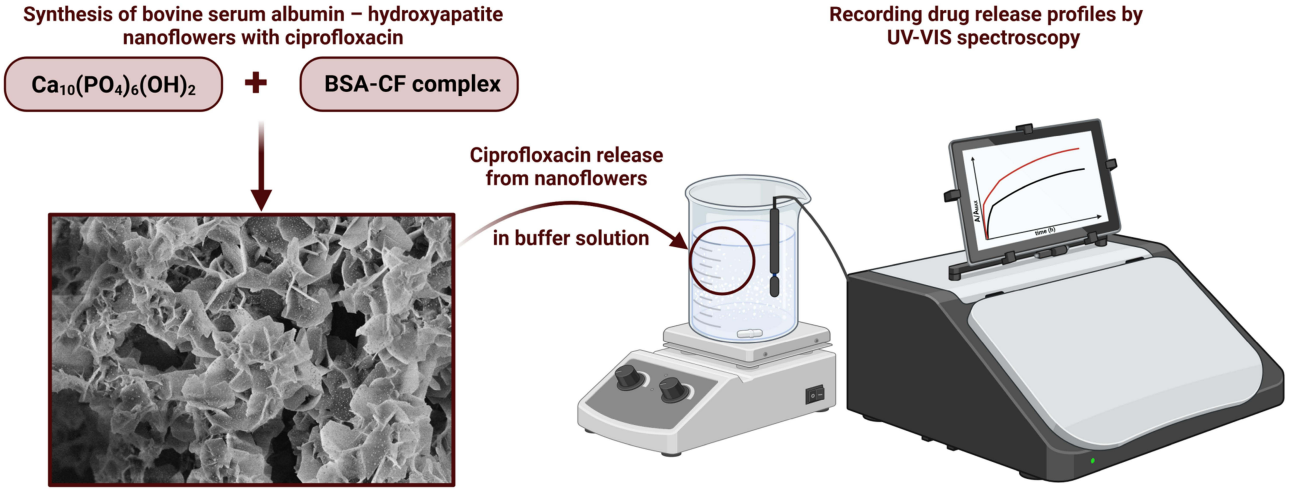

antibiotic resistance may contribute to the death of up to 10 million people.[16] Therefore, new treatment strategies are urgently needed, such as the original approach to local delivery of antimicrobial drugs to infected sites presented in this manuscript. In this paper, we present the synthesis and characterization of hybrid nanoflowers based on bovine serum albumin (BSA) and hydroxyapatite (HA) for DDS of ciprofloxacin, a wide-spectrum antibiotic used in osteomyelitis treatment. Considering that bones are organic–inorganic composites (osteoid and HA), hybrid nanoflowers composed of BSA (organic) and HA (inorganic) are very interesting as bone treatment materials.

Hybrid organic–inorganic flower-like structures were characterized for the first time in 2012 by Ge and coworkers.[17] They described protein-copper (II) phosphate (V) micrometer-sized structures, composed of petals forming hierarchical assemblies and called them *hybrid nanoflowers*. The petals were made of nanosized copper phosphate crystals "glued" by protein molecules, and their thickness was measured in nanometers. Following the pioneers in this field, the name *hybrid nanoflowers* has been used by other researchers in subsequent published reports, and we also describe structures obtained in this study as hybrid nanoflowers. After the first report, where copper ions and phosphate buffer were used to form nanoflowers with different proteins, further studies with copper and other ions, including cobalt, calcium, zinc, iron and manganese, were carried out.[18–33] However, compared to nanoflowers synthesized with copper ions, they are still in the minority. Taking into account the potential applications of hybrid nanoflowers in biomedicine, the usage of nontoxic metal ions must be considered. Copper is a trace element with a required intake of ca. 1–10 mg per day. Although copper ions are essential for many biological processes,[34] excess copper shows cellular toxicity.[35] Ingestion of more than 1 g of copper sulfate causes symptoms of poisoning and may be lethal. For comparison, 1 g per day is the recommended amount of calcium intake, which can be more than doubled in specific cases. Calcium is an essential element for building bones and teeth. Calcium homeostasis in plasma plays a vital role in the regulation of hormonal secretion, vascular activities[36] and other processes, such as cell growth, cell migration, and neuronal excitability.[37] Therefore, we used calcium as a nontoxic ion to form hybrid nanoflowers with BSA in phosphate-buffer saline (PBS). Calcium-incorporated nanoflowers were synthesized for the first time with α-amylase by Wang et al.[38] Since then, several biomolecules have been used to develop Ca-based nanoflowers, including sericin,[39] elastin-like polypeptides,[40] chymotrypsin,[41] α-acetolactate decarboxylase,[42] chloroperoxidase,[43] chitosan[44] and tandem systems such as concanavalin A-invertase.[45] In all of them, calcium triphosphate was the inorganic component, which was proven by X-ray diffraction.

As mentioned before, in this paper, a calcium salt solution was used together with BSA to form hybrid nanoflowers in the presence of phosphate ions. BSA was chosen by us as a model for human serum albumin (HSA), which is the best choice for

building hybrid protein-inorganic delivery systems, as HSA is the most abundant protein in human plasma. In contrast to HSA, BSA is easily available and inexpensive; therefore, it is used in experiments instead of HSA. Moreover, serum albumin has recently found application in enhancing the integration of biomaterials with bone tissue, with research demonstrating its significance in the context of bone repair and regeneration.[46] Albumins are also attractive because they are nontoxic, nonimmunogenic, soluble in water, temperature resistant and bind weakly and reversibly to both cations and anions, which is beneficial for delivery systems.[47,48] According to recent literature reviews, albumins can transport different ions (Na^+, K^+, Ca^{2+}) and (bio)molecules, including peptides, hormones, antibodies and drugs, such as ciprofloxacin.[49–51] Ciprofloxacin (CF) is one of the most important and widely used antibiotics, belonging to the fluoroquinolone family.[52] It has bactericidal activity against most strains of gram-negative and some gram-positive bacteria.[53–55] Due to good pharmacokinetic properties and the ability to achieve higher concentrations in tissues than in plasma, ciprofloxacin is widely used to treat respiratory, urinary tract and gastrointestinal infections.[56] It is also used to treat skin, bone and joint infections.[57] Ciprofloxacin forms complexes with BSA, as proven by different methods.[58–60] This feature, together with the ability of BSA to form Ca-based hybrid nanoflowers, encouraged us to study such a system as a potential DDS for ciprofloxacin. Our experiments showed that precipitates obtained from PBS buffer solutions containing BSA and Ca^{2+} at specific concentrations are composed of interconnected BSA and hydroxyapatite ($Ca_{10}(PO_4)_6(OH)_2$) nanoparticles forming flower-like structures. Hydroxyapatite (HA) is one of the most studied biomaterials and has been used as a drug and protein carrier, which has been summarized in recent reviews.[61–64] Hybrid structures with HA as an inorganic component and different organic molecules were described in.[65–69] However, to the best of our knowledge, this is the first paper presenting the synthesis of hybrid HA-BSA nanoflowers and studying their usage as drug delivery systems.

In this article, the synthesis of hybrid nanoflowers based on bovine serum albumin and hydroxyapatite was presented, and the obtained hybrid structures were tested as ciprofloxacin delivery systems. Flower-like hierarchical structures were visualized using scanning electron microscopy (SEM). Attenuated total reflectance Fourier transform infrared (ATR-FTIR) spectroscopy and thermogravimetric analysis (TGA) were applied to confirm the embedding of ciprofloxacin into the nanoflower structure. X-ray diffraction (XRD) studies proved the presence of nanocrystalline HA. To determine the release profiles of ciprofloxacin from nanoflowers, UV–Vis spectroscopy was applied, and the process kinetic parameters were determined. Moreover, antibacterial activity was demonstrated against pathogenic *Staphylococcus aureus* and *Pseudomonas aeruginosa*.

To the best of our knowledge, this is the first paper presenting the synthesis and characterization of hybrid nanoflowers based on hydroxyapatite. Moreover, this is the first paper in which enzyme-based nanoflowers were used as a potential DDS for ciprofloxacin, a drug of choice in osteomyelitis treatment. The specific structure of hybrid nanoflowers enables a high load of CF – up to 60% (wt.). Moreover, hybrid nanoflowers composed of BSA and HA nanocrystals resemble bone structures and show microporosity and rough surfaces, which are beneficial for the local treatment of bone infections, as such structures can support the development of extracellular matrix and cell colonization, leading to faster tissue regeneration.

Materials and Methods

Chemicals

Ciprofloxacin ≥98.0% (HPLC); Batch # 0000118430, albumin from bovine serum, minimum 98% electrophoresis; Batch # 017K0722 were purchased from Merck (Darmstadt, Germany) and used without further purification. Drug and enzyme solutions were prepared in 10 mM phosphate-buffered saline (PBS), pH 7.4. PBS buffer was prepared from sodium chloride, NaCl and disodium phosphate, Na_2HPO_4 from POL-AURA (Warsaw, Poland), potassium chloride, KCl and potassium phosphate monobasic KH_2PO_4 from Merck (Darmstadt, Germany). Calcium nitrate tetrahydrate, $Ca(NO_3)_2{\cdot}4H_2O$, was purchased from CHEMPUR (Piekary Śląskie, Poland). Acetate buffer (10 mM, pH 5.0) was prepared from acetic acid 99.5%-99.9% and sodium acetate trihydrate from Avantor Performance Materials Poland (Gliwice, Poland). Water was purified by reverse osmosis in the (RO) Milli-Q station, and its resistivity was 18.2 MΩ·cm.

Instrumentation

Electrochemical characterization was carried out in a three-electrode electrochemical system using a potentiostat/galvanostat PalmSens system (Houten, The Netherlands). A platinum grid was used as the counter electrode, and a saturated calomel electrode served as the reference electrode. Glassy carbon electrodes (GCEs) with a diameter of 2 mm were used as the working electrode. The surface of the working electrodes was polished on a water-moistened pad with alumina powder (Al_2O_3). Next, the working electrode was rinsed with DI water and wiped with a dust-free cleaning wipe. The reference and platinum electrodes were also rinsed several times with DI water.

The spectroscopic analyses were conducted by using an S-I-Photonics-Model 440 UV/Vis spectrophotometer in the wavelength range from 230 to 400 nm. The FTIR spectra were recorded on a Thermo Scientific Nicolet iS10 FTIR spectrometer (Thermo Fisher Scientific, Waltham, MA, USA) in the range 3650–650 cm^{-1} using a PIKE Technologies MIRacle (Madison, WI, USA) accessory equipped with a ZnSe crystal designed for the single reflection horizontal ATR technique. SEM images of the nanoflowers were taken using a ZEISS CrossBeam 540 scanning electron microscope. Samples were Au-sputtered before measurements. All of these measurements were carried out at room temperature.

Thermogravimetric measurements were carried out by using a Netzsch STA 449 F1 thermal analyzer in the temperature range from 40°C to 850°C in an argon atmosphere, with a uniform heating rate of 5°C/min for all samples.

Samples were analyzed with the X-ray diffraction (XRD) method using an X'Pert Pro MPD system with CuKα radiation. The measurements were acquired over a 2θ range of 10–80° at room temperature with powdered samples. The mean crystallite dimensions were calculated based on the (002) and (211) reflexes using High Score software.

Methods

Synthesis of Hybrid Nanoflowers

Hybrid nanoflowers were synthesized with and without ciprofloxacin. In the first approach, 50 mL of 0.1 mg/mL BSA in PBS solution (10 mM, pH 7.4) was added to 47.5 mL of 0.5 mM ciprofloxacin in PBS solution (10 mM, pH 7.4). Next, 2.5 mL of 32 mM calcium nitrate tetrahydrate water solution was added, followed by incubation at room temperature for 24 h. After incubation, the white precipitate was centrifuged (13.4k rpm for 5 minutes), rinsed with 2 mL of DI water and centrifuged again; this step was repeated two times. Next, the precipitate was dried at room temperature. Nanoflowers without ciprofloxacin were synthesized in a similar way, but instead of a ciprofloxacin solution, 47.5 mL of PBS solution (10 mM, pH 7.4) was added to the mixture. After 24 hours, essential steps to clean and dry the precipitate were repeated.

Calibration Curve Preparation

Calibration curves were plotted based on cyclic voltammetry and differential pulse voltammetry peak currents recorded for ciprofloxacin in PBS solution (10 mM, pH 7.4) at concentrations from 10 to 100 μM using a GC electrode as the working electrode. After each scan, the working electrode was cleaned by polishing on a water-moistened pad with alumina powder to avoid adsorption of the drug on the electrode surface. The calibration curves were prepared for comparison for 10–100 μM ciprofloxacin using the UV–Vis spectra in the range 230 nm – 400 nm. The calibration curves were plotted at different pH values using PBS buffer solution (10 mM, pH 7.4) and acetate buffer solution (10 mM, pH 5.0).

Ciprofloxacin Release Profiles from Nanoflowers

UV–Vis spectroscopy was employed to record ciprofloxacin release from 0.05 mg/mL nanoflowers in solutions of PBS (10 mM, pH 7.4) and acetate buffer (10 mM, pH 5.0). The release of ciprofloxacin was monitored by absorbance read-out at 270 nm (pH 7.4) and 276 nm (pH 5.0) for 21 hours. In all cases, during the recorded release profiles, the solutions were continuously stirred (550 rpm) by a magnetic stirrer.

Antibacterial Studies

Clinical isolates of *S. aureus* and *P. aeruginosa* from the Department of Molecular Virology University of Warsaw collection that were sensitive to ciprofloxacin were used in the analysis. The strains were isolated from infections in dogs. Their identification was performed using the MALDI BIOTYPER® system (Bruker), which is a microbial identification

system based on MALDI-TOF mass spectrometry. The antibiogram of the isolated strains was conducted using the VITEK-2 system (bioMérieux) and is available as ESI.

Bacteria were grown on LB-agar plates or in LB liquid medium at 37°C. All assays were carried out in triplicate.

For the agar disk diffusion method, overnight cultures of bacteria were spread on LB agar plates. Next, diffusion disks (5 mm blank discs, BIOMAXIMA) soaked with 25 µL of NF-CF, CF or NF (all at 1 mg/mL concentration) suspensions were placed on the plate surfaces. Plates were incubated for 16 h, and bacterial growth inhibition zones were measured and analyzed.

For the bacterial colony counting method, the same overnight cultures were used. To 0.9 mL of fresh LB medium, 100 µL of bacteria was added to obtain final colony-forming units (CFU^{-1}) of approximately 5×10^7. Immediately, 25 µL of NF-CF, CF or NF (all at 1 mg/mL concentration) suspensions were added to the bacteria. The control sample was supplemented with 25 µL of water. Samples were incubated with shaking at 37°C. At time 0 and after 2 h of incubation, 100 µL of sample was collected for CFU analysis. The serial dilutions in PBS were prepared, and 100 µL of every dilution was spread on LB-agar plates. After 16 h of incubation, colonies formed on the agar plates were counted, and $CFU \times mL^{-1}$ was calculated.

Results

Electrochemical and Optical Determination of Ciprofloxacin

As ciprofloxacin is electrochemically active and its solutions absorb light in the UV–Vis range, it was possible to analyze the CF by cyclic voltammetry (CV), differential pulse voltammetry (DPV) and UV–Vis spectroscopy.

First, the electrochemical properties of CF were evaluated. Ciprofloxacin anodic oxidation is a 2-electron transfer process.[52,70] In the cyclic voltammograms, one irreversible oxidation peak at approximately 1 V was recorded, increasing with CF concentration in the range of 10–100 µM (Figure 1A). The upper concentration of the linear range equal to 100 µM was limited by the low solubility of CF. Based on the CV scans, the calibration curve for ciprofloxacin in PBS solution (10 mM, pH 7.4) was plotted (Figure 1B). The calculated slope S_{CV} was equal to 5.2±0.3 nA/µM, with a good correlation coefficient $R^2 = 0.992$.

To improve the peak resolution, differential pulse voltammetry (DPV) was used. Solutions of 100 µM ciprofloxacin in buffers of pH 7.4, 7.0, 6.0 and 5.0 were first measured. As shown in Figure 2A,2C, when the pH value decreased, the potential of the oxidation peak was shifted toward more positive potentials. Depending on the pH of the solution, protonation and deprotonation of the carboxylic group in the ciprofloxacin structure also contributes to the change of peak potential, which was described in.[51,69] DPV scans (Figure 2A,2B) for 10–100 µM ciprofloxacin in PBS solution (10

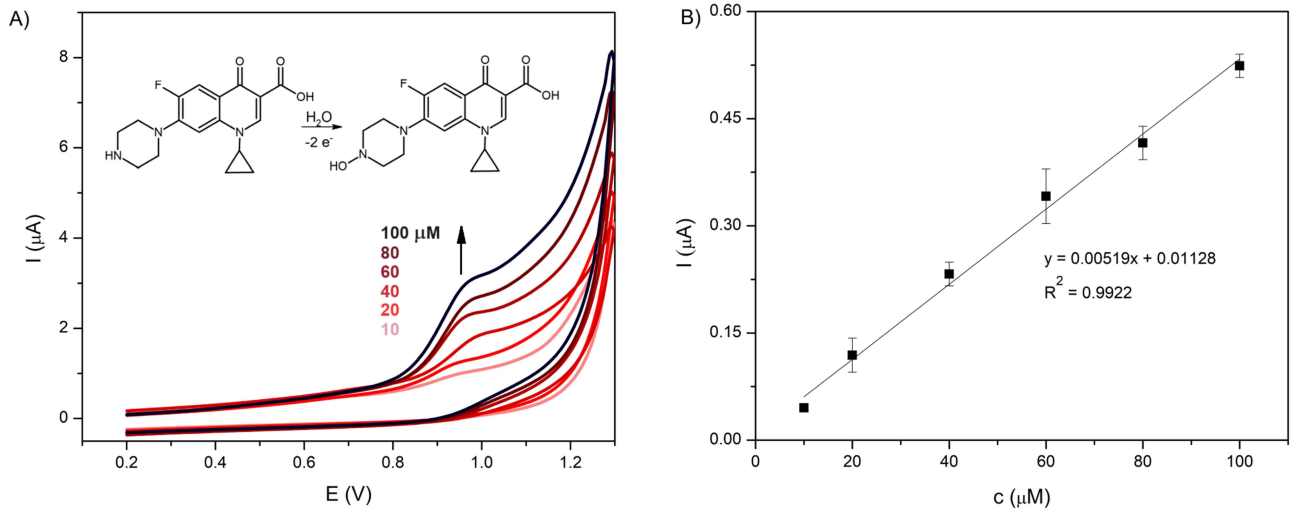

Figure 1 (**A**) Cyclic voltammograms recorded for 10–100 µM ciprofloxacin in PBS solution (10 mM, pH 7.4). The potential window from 0.2 to 1.3 V, scan rate 0.1 V/s. (**B**) Calibration curve based on CV scans.

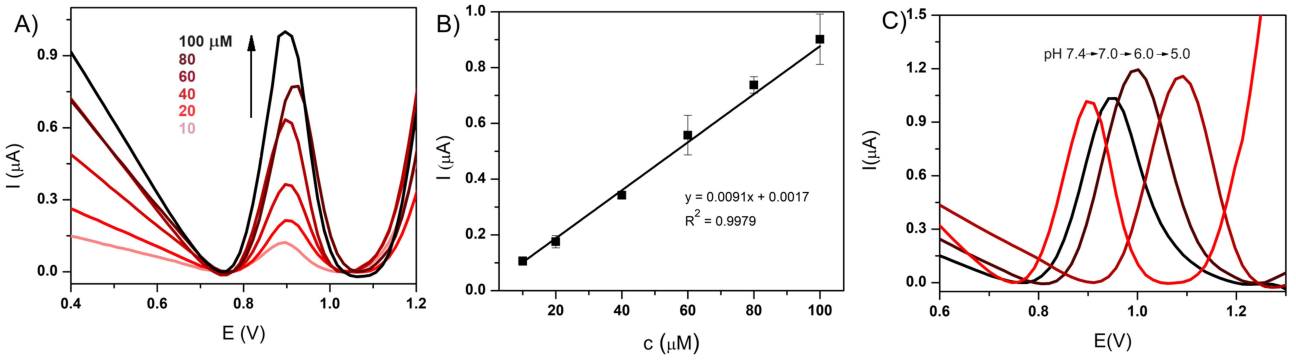

Figure 2 (**A**) Differential pulse voltammograms for 10–100 µM ciprofloxacin in PBS solution (10 mM, pH 7.4). Potential window 0.4–1.2 V. (**B**) Calibration curve based on DPV scans. (**C**) DPV plots for 100 µM ciprofloxacin in varying pH buffer values (7.4, 7, 6 and5).

mM, pH 7.4) were employed to obtain the calibration curves (Figure 2B,2C). The slope of the calibration curve of S_{DPV} was nearly two times higher than that of S_{CV} and was equal to 9.1±0.8 nA/µM, with better linearity (R^2 = 0.998).

In the second approach, UV–Vis spectroscopy was applied to determine CF in the samples. Spectra in the range of 230–400 nm were recorded for ciprofloxacin in PBS, pH 7.4, and acetate buffer solution, pH 5.0 (Figure 3A). The UV–Visible absorbance spectrum of CF in PBS solution (10 mM, pH 7.4) shows three maxima at 270 nm, 323 nm and 334 nm, and at pH 5.0, the bands were shifted to 276, 315 and 327 nm. The maximum at the lowest wavelength is connected with the π to π* electronic transition in the C=C-C=O group. The shift from 276 nm to 270 nm corresponds to the π to π* electronic transition, which originates from deprotonation of the carboxylic acid group and is related to the increasing pH of the solution. The maxima corresponding to the n to π* electronic transitions were shifted from 315 nm to 323 nm at pH 7.4 and from 327 nm to 334 nm at pH 5.0.[71] The wavelength corresponding to the maximum absorbance of CF was chosen for analysis. The maximum of the first absorption band for CF measured at pH 7.4 was observed at 270 nm and was redshifted to 276 nm in the spectrum recorded at pH 5.0. The calibration curves shown in Figure 3B were plotted as the maximum absorbance vs CF concentration for the two studied pH buffers. A linear relationship was obtained in the range of 10–100 µM. The sensitivities obtained for 7.4 and 5.0 buffer were similar and equal to 0.0175±0.0001/µM and 0.0178±0.0001/µM, respectively. The correlation coefficients were similar and equal to 0.998 (pH 5.0) and 0.992 (pH 7.4).

Calibration curves for CF were successfully obtained with a linear relationship in the range of 10–100 µM for both methods used, that is, DPV and UV–Vis. Due to the low solubility of ciprofloxacin at a pH of approximately 7.4, it was

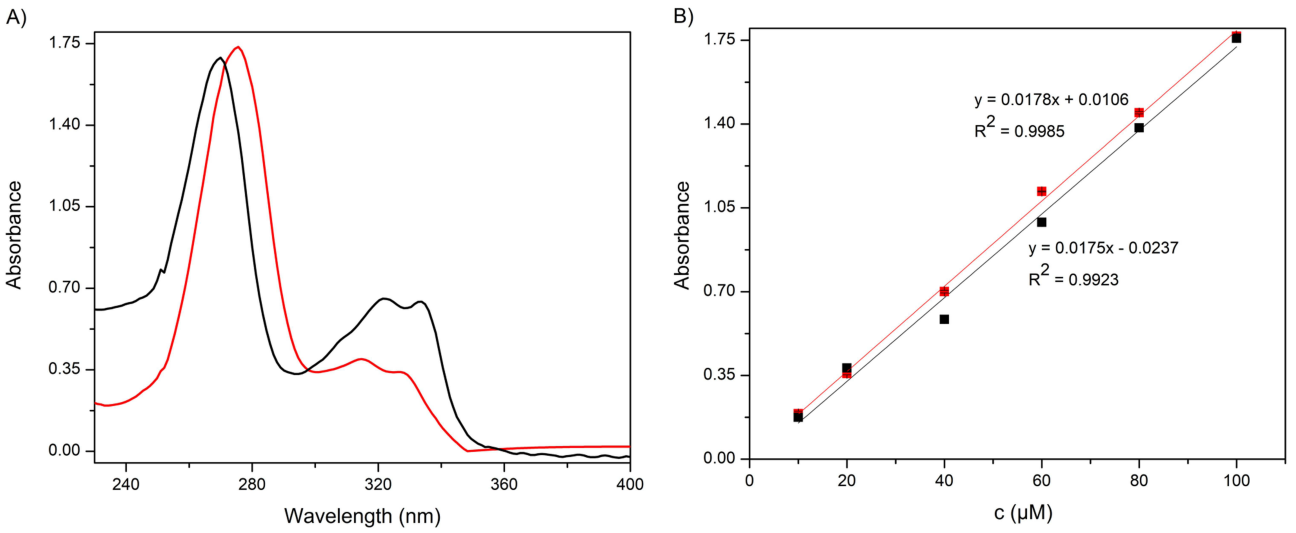

Figure 3 (**A**) UV–Vis spectra for 100 µM ciprofloxacin solutions in 10 mM PBS pH 7.4 (black) and in 10 mM acetate buffer pH 5.0 (red). (**B**) Calibration curves based on UV–Vis spectra.

not possible to obtain a stable solution with a concentration above 100 µM. For the electrochemical method (DPV), the slope of the calibration curve S_{DPV} was equal to 9.1±0.8 nA/µM, with linearity R^2 = 0.998. The sensitivity of UV–Vis measurement was equal to 0.0175±0.0001/µM. The correlation coefficients were similar for both methods: 0.998 for DPV and 0.992 for UV–Vis. It is difficult to compare the sensitivity of these two methods, as the slope is given with different units. However, it can be estimated that in the studied concentration range, the recorded signal increased ca. 10% of its maximum value with a concentration change of 1 µM. This means that these two methods can be successfully used for CF determination in different samples.

Characterization of Hybrid Nanoflowers

Hybrid nanoflowers (NFs) were synthesized by mixing bovine serum albumin in PBS solution (10 mM, pH 7.4) with calcium nitrate tetrahydrate solution. After 24 h, the white precipitate was centrifuged and dried at room temperature. For the formation of nanoflowers, the concentration of metal ions and biomolecules is important because it has a significant effect on nanoflower morphology; thus, we strictly repeated the protocol published elsewhere.[72] Hybrid nanoflowers incorporating ciprofloxacin (NF-CF) were synthesized in the same manner, mixing BSA with CF in the first step. To confirm flower-like hierarchical structures, the precipitate was imaged by scanning electron microscopy (SEM, Figure 4).

SEM images confirmed that during the synthesis, hybrid nanoflowers were obtained, with a size of ca. 1–2 µm (Figure 4A–D). The thickness of petals forming flowers was in the range of several nanometers. As the sample was Au-sputtered before SEM imaging, it was not possible to determine the correct values of petal thickness. The SEM images also revealed that the addition of drug had no significant impact on nanoflower morphology (Figure 4C and D). Moreover, petals of nanoflowers synthesized with ciprofloxacin were better separated than in its absence and were sharper-edged. Hydroxyapatite was the inorganic component of the hybrid nanoflowers, as was proven by the XRD and TGA-DSC analysis described in the next parts of the manuscript. The mechanism of BSA-hydroxyapatite hybrid NF formation is depicted in Figure 5.

XRD Analysis of Nanoflowers

To specify the inorganic phase in the nanoflowers, X-ray diffraction (XRD) analysis was performed. The diffractogram presented in Figure 6 clearly shows that the inorganic phase in the synthesized nanoflowers is hydroxyapatite ($Ca_{10}(PO_4)_6(OH)_2$).[73] The small reflex centered at 2Θ=22.8° confirms the presence of BSA molecules in the sample.[74] Hydroxyapatite

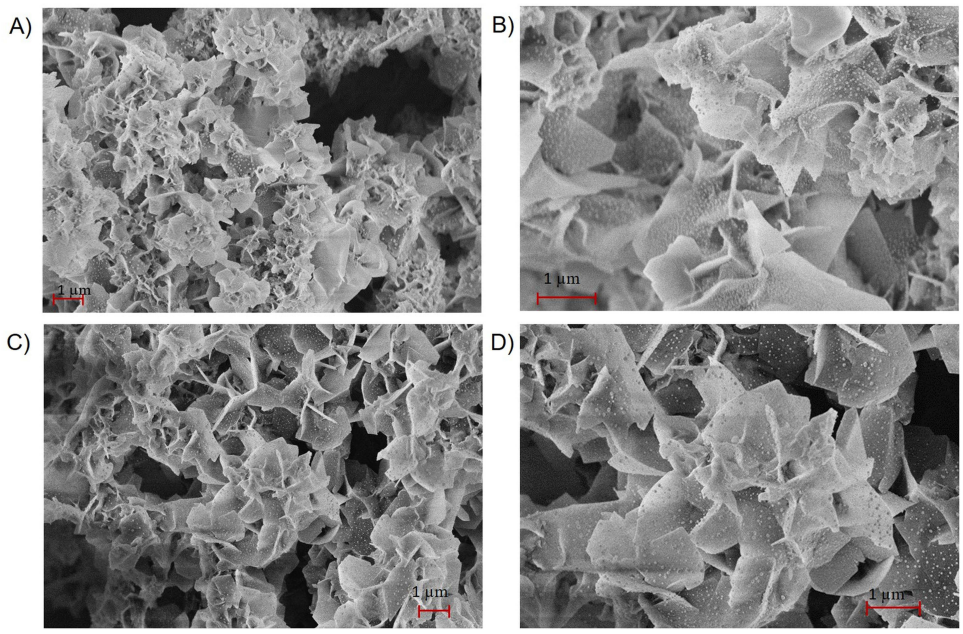

Figure 4 (**A** and **B**) SEM images of hybrid nanoflowers synthesized without ciprofloxacin. (**C** and **D**) SEM images of hybrid nanoflowers synthesized with ciprofloxacin.

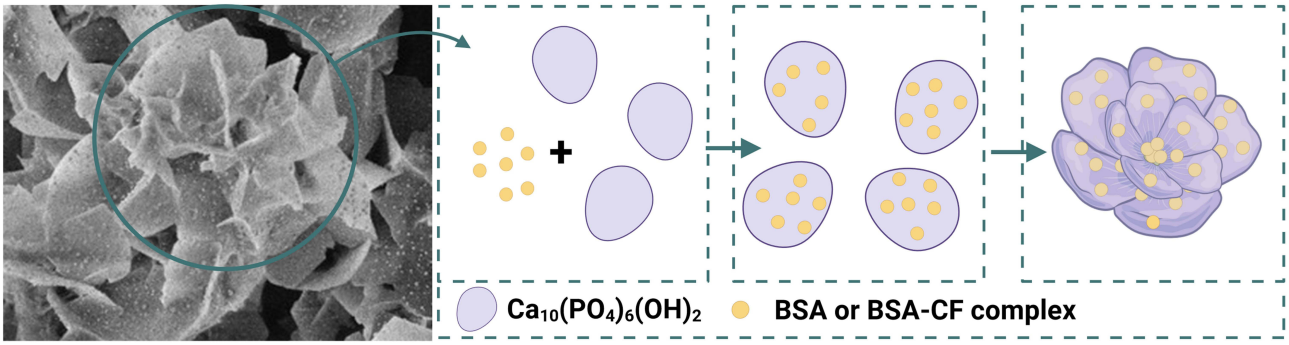

Figure 5 Illustration of the formation process of bovine serum albumin – hydroxyapatite nanoflowers. Created with BioRender.com.

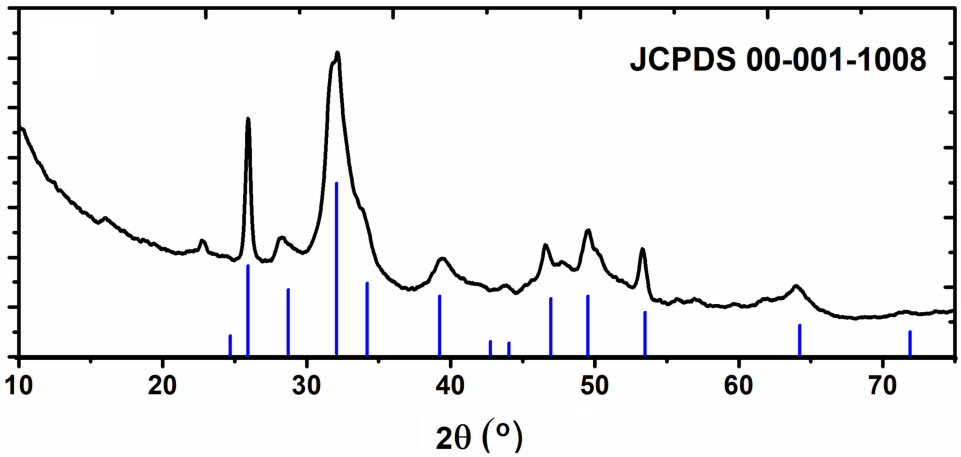

Figure 6 X-ray diffractogram of nanoflower sample in comparison to XRD pattern of hydroxyapatite (according to JCPDS 009–0432).

(HA) crystalizes mostly in hexagonal (space group P63/m) or, to a lesser extent, monoclinic crystal systems (P21/b space group). The diffractogram presented in Figure 6 corresponds well to the hexagonal hydroxyapatite crystal pattern (JCPDS 009–0432). Broadening of the reflexes is characteristic for nanosized crystallites. The most intense reflex, located at 2Θ = 32.0°, refers to the (211) plane. The reflex at 2Θ = 25.9° matching the (002) plane is sharper than the other reflexes. This means more preferable crystal growth along the c-axis. Using dedicated software, the size of the hydroxyapatite crystallites was calculated utilizing broadening of 25.9 and 32.0° reflexes. The determined length of the HA nanocrystals was 20.4±2.0 nm, and the width was 6.0±0.5 nm. The results confirmed the preferential growth of HA nanocrystals along the c-axis, leading to elongated structures. Moreover, the calculated size of the HA crystallites is consistent with the SEM results, which revealed that the thickness of the petals forming nanoflowers is measured in nanometers.

ATR-FTIR Analysis of Nanoflowers

Attenuated total reflectance Fourier transform infrared spectroscopy was used to identify the functional groups in the nanoflower structure and to confirm the embedding of ciprofloxacin. Figure 7 presents the spectra of bovine serum albumin (BSA), ciprofloxacin (CF), nanoflowers synthesized without drug (NF) and nanoflowers synthesized with ciprofloxacin (NF-CF).

The ATR-FTIR spectrum of hybrid nanoflowers synthesized without ciprofloxacin shows characteristic amide bands: wide at 3308 cm^{-1} (amide A band), at 1653 cm^{-1} (amide I band) and at 1543 cm^{-1} (amide II band).[75] An intense,

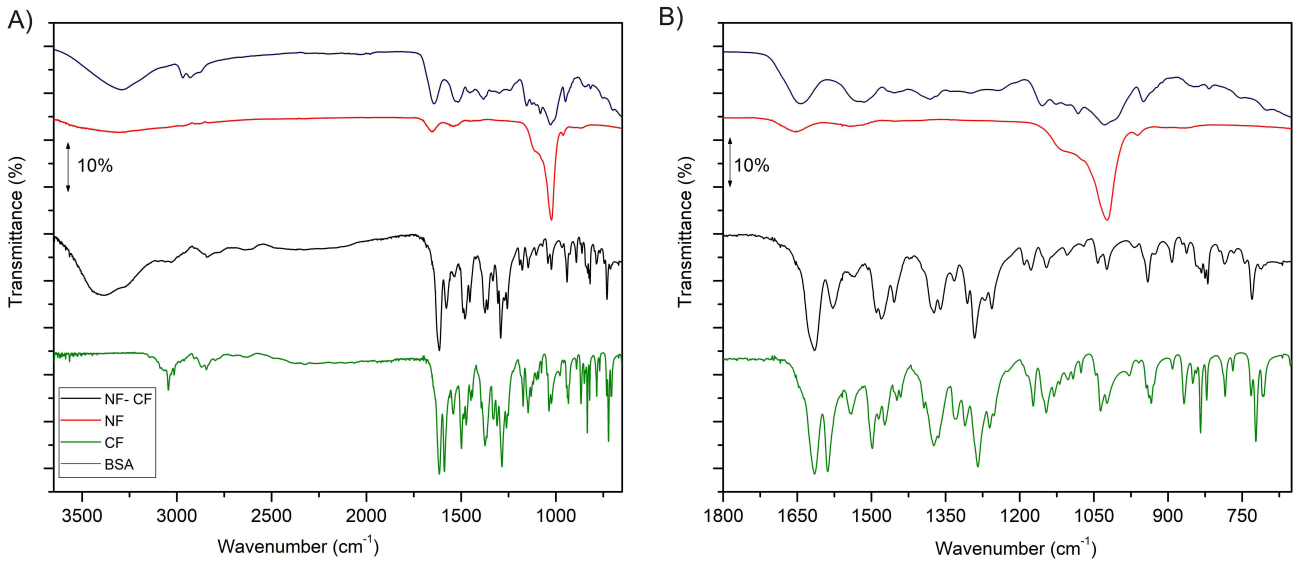

Figure 7 ATR-FTIR spectra of BSA, nanoflowers synthesized without ciprofloxacin, with ciprofloxacin and ciprofloxacin in the range 3650 cm^{-1} – 650 cm^{-1} (left), ATR-FTIR spectra in the range 1700 cm^{-1} – 650 cm^{-1} (right).

characteristic band for the stretching vibration of the phosphate group (PO_4^{3-} ν_3) at 1023 cm^{-1} and a less intense band at 961 cm^{-1} (PO_4^{3-} ν_1) are also present.[76] These bands confirm the presence of bovine serum albumin and phosphates in the structure of the nanoflower. The ATR-FTIR spectrum of the nanoflowers with ciprofloxacin shows numerous characteristic bands of ciprofloxacin, which confirms its presence in the hybrid nanoflower structure. It includes a band at 3029 cm^{-1} corresponding to C-H stretching vibrations of the aromatic ring, a 2838 cm^{-1} band related to C-H symmetric and asymmetric stretching vibrations of the methylene groups, a band at 1615 cm^{-1} due to C=O stretching vibrations of the carbonyl group (at the C4 position of the quinoline ring) and bands in the range 1540 cm^{-1} – 1450 cm^{-1} corresponding to symmetric and asymmetric stretching vibrations between carbon atoms in the aromatic ring.[77] Characteristic bands for stretching vibrations of the phosphate group at 1023 cm^{-1} and 961 cm^{-1} are also present in the spectrum, as well as the amide bands at 3301 cm^{-1}, 1653 cm^{-1} and 1533 cm^{-1}. Overall, the ATR-FTIR analysis confirms the presence of ciprofloxacin in the synthesized hybrid nanoflower structure.

Thermogravimetric Analysis of Nanoflowers

XRD analysis confirmed the presence of hydroxyapatite in the synthesized nanoflowers, while FTIR was used to prove the presence of all constituents of the NF and NF-CF samples. As BSA-hydroxyapatite NFs and NF-CFs were obtained for the first time, additional studies using thermogravimetric analysis (TGA) with differential scanning calorimetry (DSC) were carried out. TGA-DSC analysis further confirmed the presence of HA and BSA in the NF sample and proved CF incorporation into the NF-CF sample. Thermogravimetric measurements of the CF, NF and NF-CF samples were carried out in an argon atmosphere in the temperature range from 40°C to 850°C, and the obtained results are presented in Figure 8.

Figure 8A shows the thermogravimetric (TG) and derivative thermogravimetric (DTG) curves recorded for ciprofloxacin. The distinct mass loss observed between 250–350°C and 350–500°C in the TG curve, with maxima of 340°C and 412°C, respectively, in DTG, could be attributed to ciprofloxacin decomposition with the release of the following molecules: acetylene, ethylene, hydrogen fluoride, hydrogen and mono nitrogen oxide, which was reported elsewhere.[77] As shown in Figure 8B, the process is endothermic, with an energy consumption of ca. 5.5 mW/mg. Above the temperature of ca. 450°C, sample melting is observed, as small endothermic peaks are present in the DSC curve with no mass loss in the TG. The total mass loss of free ciprofloxacin was equal to 69%.

Figure 8C shows the TG and DTG curves obtained for nanoflowers without ciprofloxacin. In the temperature range up to 150°C, the observed mass loss in TG is associated with surface water desorption, with maxima ca. 100°C in the DTG

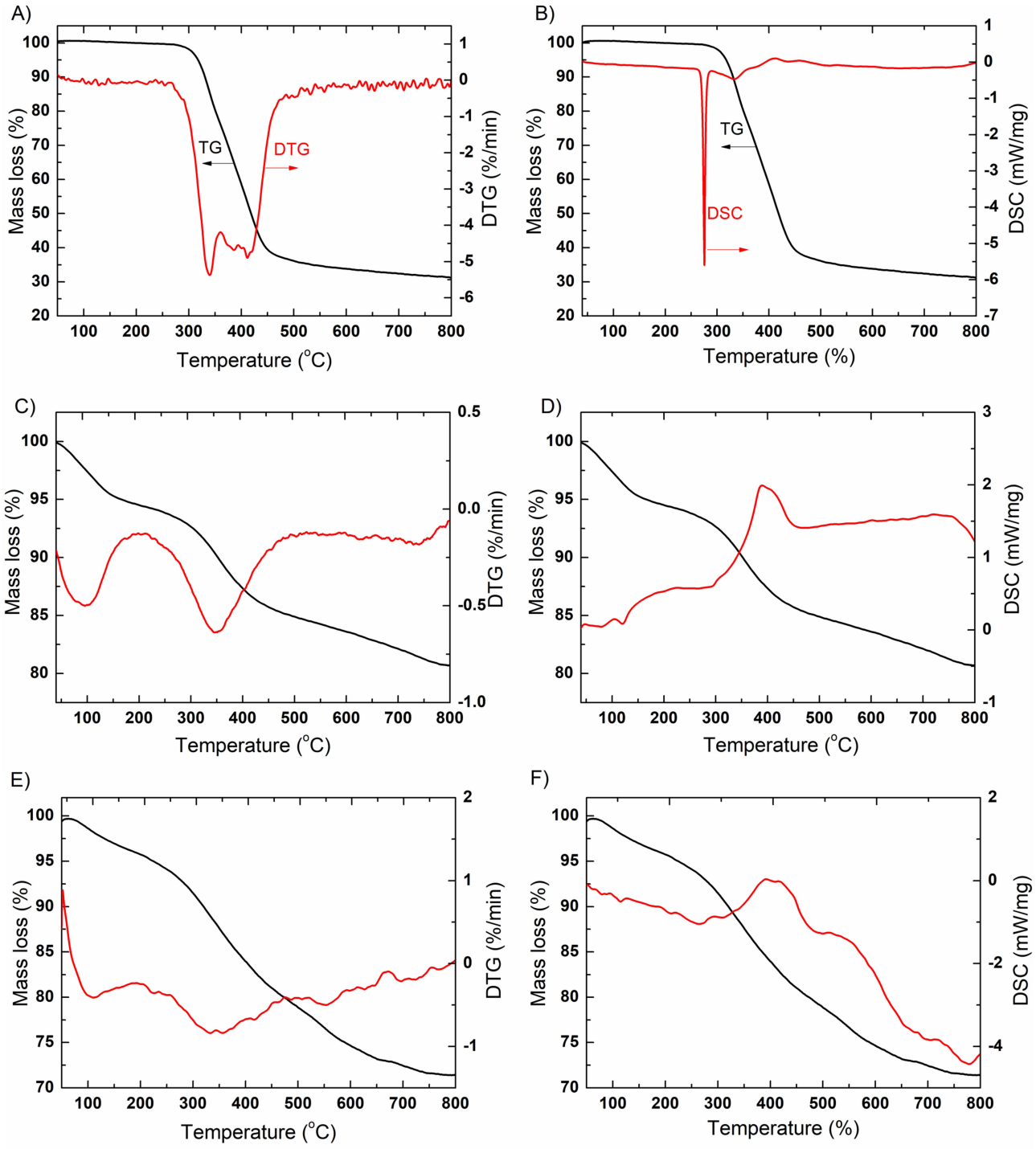

Figure 8 TG and DTG curves of CF (**A**), NF (**C**) and NF-CF (**E**). DSC curves of CF (**B**), NF (**D**) and NF-CF (**F**).

curve. A higher mass loss was detected in the temperature range from 200°C to 500°C, with a maximum at 350°C. Similar observations were reported by Kollath et al for BSA decomposition.[78] In the same temperature range, hydroxyl groups from hydroxyapatite are released.[79] The last mass loss was observed in the temperature range from 500–800°C with a maximum of 750°C. The total mass loss of the nanoflowers was 18% from the initial sample. Based on this result, it can be concluded that hydroxyapatite is the major component of NF and that the protein content does not exceed 18%.

The DSC analysis shown in Figure 8D confirmed the endothermic process of water desorption and BSA denaturation (two small peaks in the range of 50–150°C). The second mass loss observed in the TG curve above 250°C occurs with energy release, as an exothermic peak is present in the DSC curve of this sample. This can be attributed to crystallization of the inorganic phase present in the sample. Figure 8D shows that the second exothermic process starts above 700°C. This is consistent with previous studies in which hydroxyapatite decomposition to oxyapatite was reported.[80]

Figure 8E shows the TG and DTG curves of NF-CF, which revealed two decomposition steps similar to those of nanoflowers without drug. The maxima can be observed at 100°C and 350°C, similar to the NF sample; however, the decomposition rates are different. As the temperature-dependent processes occurring in the NF and CF samples are revealed at similar temperature ranges, it is not possible to differentiate them in the TG/DTG. The total mass loss of the nanoflowers synthesized with ciprofloxacin was approximately 26%.

More differences can be seen in the DSC (Figure 8F) obtained for the NF-CF sample. In the NF sample, a constant energy increase is observed up to 700°C with a visible exothermic peak, which starts ca. 300°C and ends at 500°C. However, NF-CF shows a decrease in energy in the 50–300°C region, which is connected with the endothermic decomposition process of the drug. Additionally, the heat flow rate in the NF-CF sample is negative, which is a result of the addition of two processes occurring in the sample: the endothermic process of ciprofloxacin decomposition and the exothermic crystallization of the inorganic phase.

Kinetics of Ciprofloxacin Release from Nanoflowers

UV–Vis spectroscopy was applied to determine the release profiles of ciprofloxacin from the nanoflowers. Release of the drug was conducted in phosphate buffer saline solution (10 mM, pH 7.4) and in acetate buffer solution (10 mM, pH 5.0). As shown in Figure 3A, the maximum absorption shifts toward higher wavelengths in acidic environments. The maximum absorption is present at 270 nm at pH 7.4 and 276 nm at pH 5.0; therefore, these values were used for CF release monitoring in different buffers. In all cases, drug release profiles were recorded from 0.05 mg/mL nanoflowers in buffer solution, and during measurements, the solution was continuously stirred (550 rpm) by a magnetic stirrer. Data were collected for 21 hours. Figure 9 shows the release profiles of ciprofloxacin from nanoflowers in PBS (pH 7.4) and acetate buffer (pH 5.0) solutions. The release profiles are presented as the mean of three independent release curves with standard deviation.

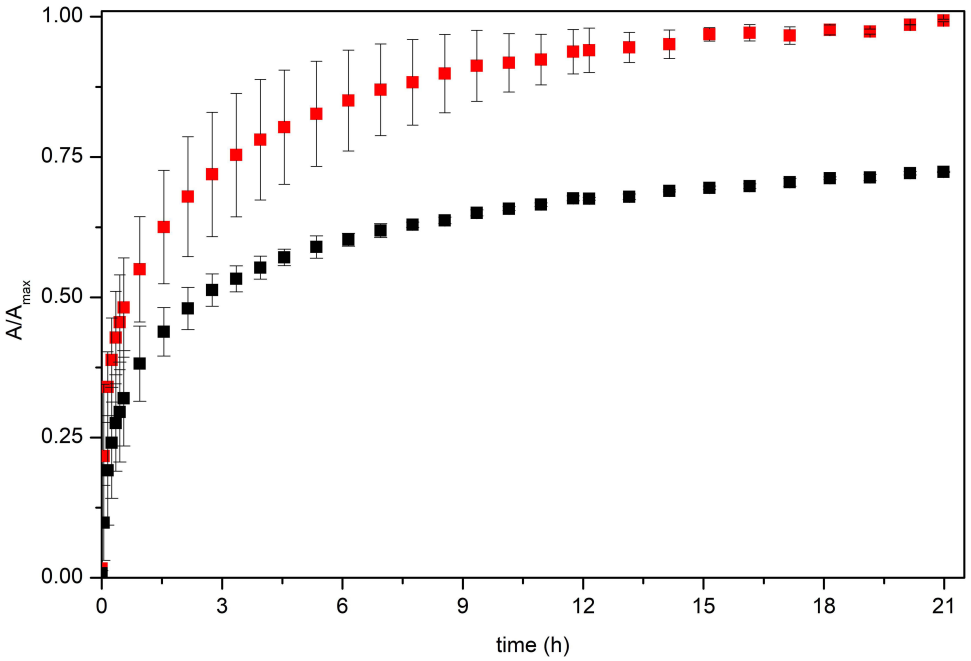

Figure 9 Release profile of ciprofloxacin from NF-CF (0.05 mg/mL) in 10 mM PBS pH 7.4 (black) and in 10 mM acetate buffer pH 5.0 (red).

The curves show the release (in %) of CF from nanoflowers over time. The release drug profiles were nonlinear. In the first hour, approximately 50% of the drug was released from the nanoflowers, and another 30% was released in the next four hours. Fourteen hours after starting release, no significant changes in absorbance values were observed (plateau). Based on the calibration curve, the total ciprofloxacin concentration in PBS solution was calculated to be 101.05 ± 1.70 μM. A similar release profile was recorded in acetate buffer solution at pH 5.0. However, in this case, the maximum concentration was higher than that in solution at pH 7.4. According to the A_{max} values, the ciprofloxacin concentration reached in acidic solution was calculated to be 126.68 ± 6.25 μM. This is 25.36% more released ciprofloxacin than at pH 7.4. This is probably because ciprofloxacin solubility depends on pH, and the solubility profile has a "U" shape, with minimum solubility at approximately pH 7 and higher solubility below 5 and above 10.[81]

In compliance with the literature, 1 to 1.5 h after administration of ciprofloxacin, the mean concentrations in serum were 4.07–4.29 μM, 7.85–8.72 μM and 10.29–12.71 μM after 250, 500 and 750 mg doses, respectively.[82] Based on the calculated ciprofloxacin concentration after release from 0.05 mg/mL nanoflowers in PBS solution per 0.001 mg/mL (1 mg/l), the drug concentration was equal to 2.02 μM. This means that with appropriately increasing concentrations of nanoflowers, achieving therapeutic ciprofloxacin concentrations could be possible.

Then, to determine the kinetics of ciprofloxacin release from the nanoflowers, each of the release curves was fitted to the following kinetic models: zero-order, first-order, Higuchi and Korsmeyer-Peppas. At pH 7.4 and pH 5.0, the best correlation coefficients were obtained for the Korsmeyer-Peppas kinetic model, with R^2 values of 0.9578 and 0.9616, respectively. According to the model, release of the drug from the carrier is regulated by diffusion; when the value of $n < 0.49$, diffusion follows Fick's law. Based on the equations, the values of $n = 0.25$ at pH 7.4 and $n = 0.23$ at pH 5.0, ergo the release of ciprofloxacin from nanoflowers occurs by diffusion, according to Fick's law. The hybrid nanoflowers are matrix carriers (without coating), so initially, ciprofloxacin is released rapidly. Then, as the diffusion distance increases, a decrease in the rate of released ciprofloxacin is observed.[83]

We recorded two release profiles of ciprofloxacin from nanoflowers by differential pulse voltammetry and compared them to UV–Vis spectroscopy. Both methods gave satisfactory results; however, the electrochemical approach was truly time consuming due to ciprofloxacin adsorption on the working electrode and the necessity of cleaning the electrode surface before each scan. Moreover, the electrochemical approach does not allow measurements to be taken exactly at the same time for different samples, and thus, the standard deviation of such measurements was substantially higher than that for the UV–Vis method. However, the electrochemical method can be used in situations where UV–Vis fails, eg, in turbid or opaque samples.

Antibacterial Properties of Ciprofloxacin-Loaded Hybrid Nanoflowers

The agar disk diffusion method was used to study the antibacterial properties of CF-loaded hybrid nanoflowers in comparison to free drug (positive control) and bare nanoflowers (negative control) (Figure 10). *Staphylococcus aureus* and *Pseudomonas aeruginosa*, known to be sensitive to ciprofloxacin, were chosen as examples of Gram-positive and Gram-negative bacteria, respectively, recognized as the main pathogens in osteomyelitis. Microbial growth was determined by measuring the diameter of the zone of inhibition. In the case of *P. aeruginosa* plates, inhibition zones with diameters of 22±1 mm and 26±2 mm were observed when analyzing NF-CF and CF, respectively. For *S. aureus*, inhibition zones with 25±1 mm and 26±2 mm diameters were observed when analyzing NF-CF and CF, respectively. No inhibition zone was observed in the case of NF antibacterial activity analysis.

The colony counting method was used for antibiotic susceptibility of *S. aureus* and *P. aeruginosa* analysis in liquid cultures (Figure 11). The initial colony forming unit (CFU) concentration in both *S. aureus* and *P. aeruginosa* cultures was approximately 5×10^7 CFU/mL. After 2 hours of incubation, the bacterial number decreased by at least three orders of magnitude, indicating that 99.9% of bacteria were killed. In the case of NF, a small increase in CFU was observed for both bacteria, which means that NF alone did not influence bacterial growth.

Discussion

Currently, antimicrobial resistance (AMR) of bacteria is a major problem in the treatment of infectious diseases. It is mainly caused by an inappropriate, too short or too excessive use of antibiotics. Unfortunately, the number of bacterial

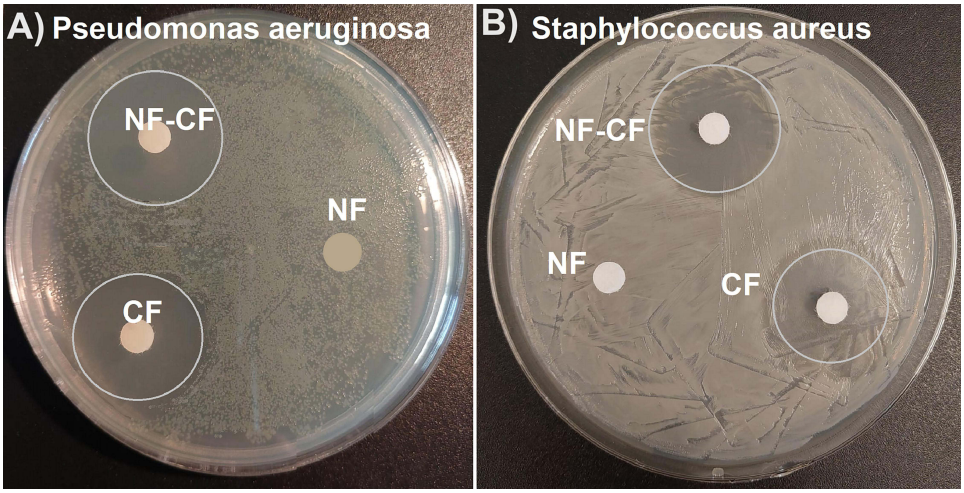

Figure 10 Susceptibility testing of *P. aeruginosa* (**A**) and *S. aureus* (**B**) using the disk diffusion method. The blank discs containing NF-CF, NF and free CF were used in the analysis. The inhibition zones (marked with circles) were present around NF-CF and CF only.

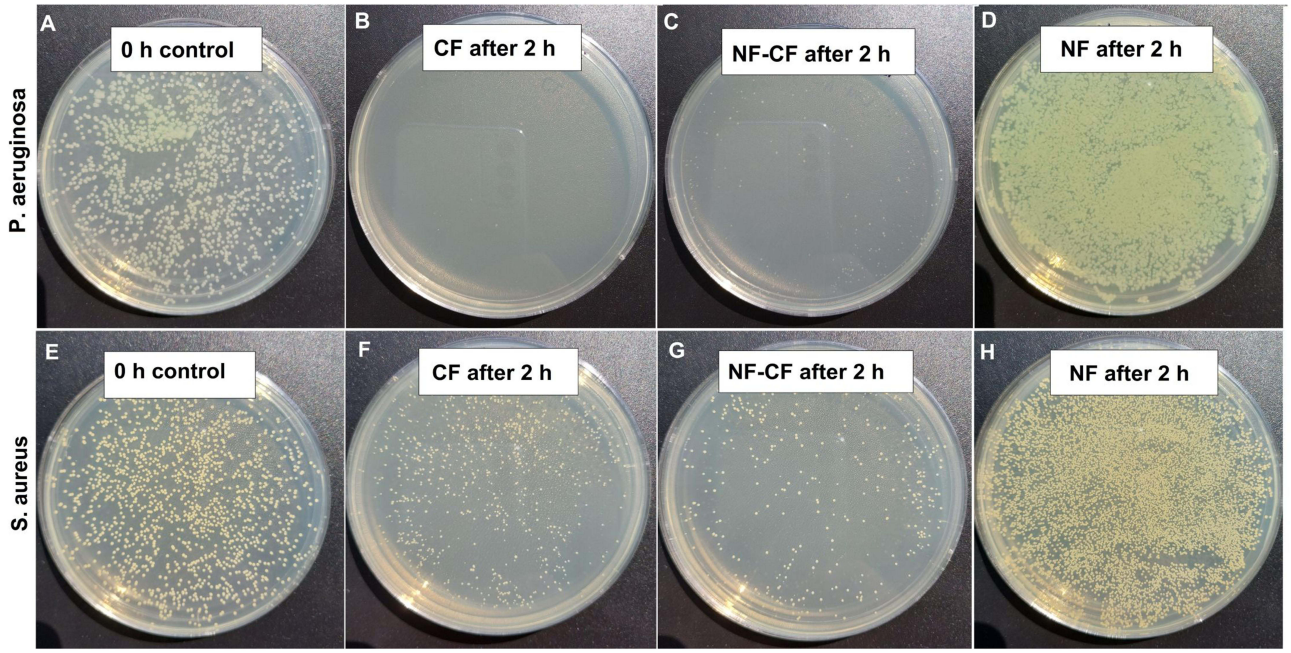

Figure 11 Antibacterial test based on CFU counting method. The initial CFU for both *P. aeruginosa* (**A**) and *S. aureus* (**E**) was around 5×10^7 CFU/mL (around 300–500 colonies on dilution 1×10^{-4}). CFU decrease of at least three orders of magnitude was observed after 2h of incubation in the presence of CF (**B** and **F**) or NF-CF (**C** and **G**). No influence -of NF on bacterial growth was observed (**D** and **H**).

strains that have antimicrobial resistance and the range of resistance continues to increase. Therefore, it is necessary to overcome this problem, and nanotechnology may provide a solution. Depending on the organic and inorganic components of hybrid nanoflowers, it is possible to develop systems with different properties needed for specific applications. Due to promising features such as one-step, environmentally friendly synthesis, biocompatible components and facile functionalization, hybrid nanoflowers are candidates for designing efficient drug delivery systems, but they are currently in the early stage of development in this field. To date, only a few complex nanoflower systems have been used for drug delivery.[84–86] Jin et al developed nanoflowers based on DNA and magnesium ions as cancer therapeutic systems for targeted dual gene silencing.[85] In another paper, doxorubicin and a photosensitizer were bound in the structure of

magnetic RNA nanoflowers. This codrug delivery system was used for targeted cancer therapy.[86] To the best of our knowledge, the synthesis of BSA-HA nanoflowers incorporating ciprofloxacin has not yet been published.

Hydroxyapatite, which is a natural component of bones and teeth, is the material of choice for different types of delivery systems (eg, nanoparticles, thin films on prostheses, cements, etc.) used for bone infection treatment,[61–69] while ciprofloxacin is one of the most commonly used antibiotics to treat osteomyelitis (bone infection). Osteomyelitis, if not properly treated, can leave bone permanently damaged. Therefore, it is important to develop new delivery systems that can be used to treat osteomyelitis in place of its occurrence. Regarding efficient local delivery systems, two things should be emphasized. First, a therapeutic concentration of drug should be achieved directly after insertion of the delivery system, avoiding excessive drug release leading to overdosage. Second, long-term sustained release at the required level should be guaranteed. Drug delivery nanosystems for the sustained release of CF have been recently summarized,[87] with a very optimistic conclusion made by the authors, who predict that nanotechnology will be a game changer in the reduction of AMR. Among others, HA structures are of major interest for treating hard tissue diseases, especially in bones and teeth.[88–90] HA microstructures with CF were obtained from alkaline solution (pH 11) containing Ca^{2+}, PO_4^{3-} and drug and heated to 90°C. The precipitate collected after cooling the reaction mixture was in the form of microparticles with sizes in the range of 0.3–1 μm and a drug load of ca. 18%.[88] However, it was shown in many reports that the drug release profile from nonmodified HA does not meet requirements in terms of time and dose.[61–63] For example, a publication cited as[65] reports HA microspheres loaded with ciprofloxacin at 0.5–2% (wt./wt.), which showed complete release of the drug within one hour. Mixing HA with natural or synthetic polymers is the main method used to overcome this issue. Polycarbohydrates, such as alginate, chitosan, and cyclodextrin polymers, are examples of biopolymers used to develop delivery systems for CF based on HA.[90–94] CF-loaded sodium alginate and HA nanorods have shown less than 40% drug release in 16 h, which was too low to achieve a therapeutic effect.[90] In contrast, sodium alginate and HA microspheres have shown burst release in the first 5 h, which was extended to 70 h by mixing such a system with gelatin.[91] The controlled CF release ability (60% in 11 days) was reported for a chitosan-alginate matrix incorporating fluorinated HA.[92] Cyclodextrins and their polymers were also used together with HA to develop a local delivery system. Cyclodextrins form inclusion complexes with many drugs, including CF. CF loading in the cyclodextrin-HA system increased 2.5-fold in comparison to nonmodified HA and displayed a burst release at the very beginning and then a progressive slowdown of the release up to 24 h.[93]

Trials with biodegradable synthetic polymers, such as polyurethane, polyvinyl alcohol and polylactide, were carried out with different results.[94–96] Polyurethane scaffolds loaded with nano-HA and CF were fabricated by in situ polymerization and simultaneous foaming methods. The developed system exhibited an initial burst release during the first 2 h and showed antibacterial activity even after two weeks of immersion in PBS.[94] Composite nanofibers made of polyurethane with nano-HA and CF were electrospun and used to produce antibacterial mats for multipurpose applications such as antibacterial packaging, filtration, and wound dressing.[95] Multistep synthesis of a delivery system based on HA nanoparticles and polyvinyl alcohol/κ-carrageenan hydrogel was presented in.[96] Studies have shown that 35% of ciprofloxacin burst release occurred during 10 h, and no burst release was seen if the HA content in the hydrogel was doubled. Special attention should be given to the results presented in[97] and[98] published by one group of authors. In both papers, HA, tricalcium phosphate, polylactide and CF in different ratios were used to create implantable scaffolds for the in vivo treatment of multibacterial bone infection. For the optimized composition, the in vivo antibacterial behavior of bone implants was observed for 8 weeks.

In addition to polymers, lipid molecules were also used to "timely arrest" CF in HA-based delivery systems, but without breakthrough results.[99,100] In both cases, the CF loading was rather low, and ca. 50% of CF was released in the first hour.

The antimicrobial tests carried out in this study clearly demonstrated the antibacterial activity of NF-CF against *Pseudomonas aeruginosa* and *Staphylococcus aureus*, two main pathogens found in osteomyelitis.[15] Both tests used, that is, the disk diffusion and plate counting methods, showed comparable results obtained for pristine CF and NF-CF, proving the release of ciprofloxacin from the studied drug delivery system at the required rate. Similar results were reported for the CF delivery system discussed above. However, in those papers, mainly *S. aureus* and *E. coli* were selected for the antimicrobial studies,[68,91,93,94] and in one paper, *P. aeruginosa* and *E. coli* were selected to verify the antibacterial properties of HA hydrogels loaded with CF.[95]

Although HA has been studied for decades, there is no report concerning simple BSA-HA nanoflower-like structures as potential drug carriers. Moreover, in all reports presenting Ca-based hybrid nanoflowers, tricalcium phosphate was proven to be an inorganic component, while among the various synthetic biomaterials, hydroxyapatite gives the best results.[61,87,97,98] Considering that bones are organic–inorganic composites (osteoid and HA), hybrid nanoflowers composed of BSA (organic) and HA (inorganic) are very interesting as bone treatment materials. Moreover, the rough surface of hybrid nanoflowers is beneficial for cell adhesion, and microsized porosity is essential for osteogenesis.

Conclusion

In this paper, we present the synthesis and characterization of hybrid nanoflowers based on BSA and HA. Formulated nanoflowers were examined as potential delivery systems for ciprofloxacin. The release of ciprofloxacin from the nanoflowers was conducted in buffer solutions at pH 7.4 and 5, and nonlinear release profiles were obtained. According to the correlation coefficient values, the kinetics of ciprofloxacin release from nanoflowers were well described by the Korsmeyer-Peppas model. Based on the calculated directional coefficients ($n < 0.49$), it was determined that the release of CF from nanoflowers occurs by diffusion. A burst release of 50% CF was recorded in the first hour, while a plateau was reached after approximately 14 hours. Hybrid nanoflowers are able to bind a significant amount of CF (up to 60% wt./wt.) due to their favorable surface-to-volume ratio and used components, which were proven to bind CF. The synthesized NF-CF showed efficient antibacterial properties against *P. aeruginosa* and *S. aureus*, which are two main pathogens responsible for osteomyelitis. Based on these results, it is anticipated that the formulated NF-CF may act as an efficient local antibiotic delivery system. There is a constant demand for new materials, including composite and nanostructured ones to support medical diagnostics and regenerative medicine therapies. Such research is aimed at maintaining a high quality of life in society, through the use of biomedical technology solutions providing access to individualized medicine and disease prevention. Due to the use of nonhazardous, biodegradable components and benign synthesis, hybrid nanoflowers are very promising drug delivery systems that could be applied in the treatment of skeletal system infections. In contrast to other reported methods, our approach is a one-step synthesis carried out at room temperature without the necessity of pH adjustment, utilizing biocompatible components. In this paper, preliminary results are reported, and additional studies will be carried out to improve the release profiles of CF and evaluate newly synthesized systems for other drugs.

Ethics and Consent Statements

All bacterial isolation swabs were performed by veterinarians during routine clinic visits. Each time, written consent from the pet's owner to take a swab and use the isolated bacteria in scientific activities was received. Documents are available on request from P. Golec (piotr.golec@uw.edu.pl).

According to Directive *2010/63*/EU of the European Parliament and Council, ethical approval is not required for the use of clinical isolates isolated from dogs.

Acknowledgments

The research was partially funded by the Nalecz Institute of Biocybernetics and Biomedical Engineering, Polish Academy of Sciences, Warsaw PL (FBW 3.3/2020). The graphical abstract and Figure 5 were created with BioRender.com.

Disclosure

The authors report no conflicts of interest in this work.

References

1. Jain KK. An Overview of Drug Delivery Systems. *Drug Delivery Sys*. 2020:1–54. doi:10.1007/978-1-4939-9798-5_1
2. Patra JK, Das G, Fraceto LF, et al. Nano based drug delivery systems: recent developments and future prospects. *J Nanobiotechnology*. 2018;16(1):71. doi:10.1186/s12951-018-0392-8
3. Stolarczyk EU, Leś A, Łaszcz M, et al. The ligand exchange of citrates to thioabiraterone on gold nanoparticles for prostate cancer therapy. *Int J Pharm*. 2020;583:119319. doi:10.1016/j.ijpharm.2020.119319

4. Stolarczyk EU, Stolarczyk K, Łaszcz M, et al. Synthesis and characterization of genistein conjugated with gold nanoparticles and the study of their cytotoxic properties. *Eur J Pharm Sci*. 2017;96:176–185. doi:10.1016/j.ejps.2016.09.019
5. Maruszak W, Stolarczyk EU, Stolarczyk K. CE method for the in-process control of the synthesis of active substances conjugated with gold nanoparticles. *J Pharm Biomed Anal*. 2017;141:52–58. doi:10.1016/j.jpba.2017.03.048
6. Dzwonek M, Załubiniak D, Piątek P, et al. Towards potent but less toxic nanopharmaceuticals – lipoic acid bioconjugates of ultrasmall gold nanoparticles with an anticancer drug and addressing unit. *RSC Adv*. 2018;8(27):14947–14957. doi:10.1039/C8RA01107A
7. Swiech O, Majdecki M, Bilewicz R. PEGylated Network Nanostructured by Gold Nanoparticles for Electrochemical Sensing of Aromatic Redox and Nonredox Analytes. *ACS Appl Polym Mater*. 2023;5(1):214–222. doi:10.1021/acsapm.2c01451
8. Swiech O, Krzak A, Majdecki M, et al. Water-soluble galactosamine derivative of β-cyclodextrin as protective ligand and targeted carrier for delivery of toxic anthracycline drug. *Int J Pharm*. 2020;589:119834. doi:10.1016/j.ijpharm.2020.119834
9. Swiech O, Majdecki M, Opuchlik LJ, Bilewicz R. Impact of pH and cell medium on the interaction of doxorubicin with lipoic acid cyclodextrin conjugate as the drug carrier. *J Incl Phenom Macrocycl Chem*. 2020;97(1–2):129–136. doi:10.1007/s10847-020-00994-z
10. Bartkowiak A, Matyszewska D, Krzak A, Zaborowska M, Broniatowski M, Bilewicz R. Incorporation of simvastatin into lipid membranes: why deliver a statin in form of inclusion complex with hydrophilic cyclodextrin. *Colloids Surfaces B Biointerfaces*. 2021;204:111784. doi:10.1016/j.colsurfb.2021.111784
11. Mierzwa M, Cytryniak A, Krysiński P, Bilewicz R. Lipidic Liquid Crystalline Cubic Phases and Magnetocubosomes as Methotrexate Carriers. *Nanomaterials*. 2019;9(4):636. doi:10.3390/nano9040636
12. Cytryniak A, Nazaruk E, Bilewicz R, et al. Lipidic Cubic-Phase Nanoparticles (Cubosomes) Loaded with Doxorubicin and Labeled with 177Lu as a Potential Tool for Combined Chemo and Internal Radiotherapy for Cancers. *Nanomaterials*. 2020;10(11):2272. doi:10.3390/nano10112272
13. Cytryniak A, Żelechowska-Matysiak K, Nazaruk E, et al. Cubosomal Lipid Formulation for Combination Cancer Treatment: delivery of a Chemotherapeutic Agent and Complexed α-Particle Emitter 213 Bi. *Mol Pharm*. 2022;19(8):2818–2831. doi:10.1021/acs.molpharmaceut.2c00182
14. Bartkowiak A, Nazaruk E, Gajda E, et al. Simvastatin Coadministration Modulates the Electrostatically Driven Incorporation of Doxorubicin into Model Lipid and Cell Membranes. *ACS Biomater Sci Eng*. 2022;8(10):4354–4364. doi:10.1021/acsbiomaterials.2c00724
15. García Del Pozo E, Collazos J, Cartón JA, Camporro D, Asensi V. Bacterial osteomyelitis: microbiological, clinical, therapeutic, and evolutive characteristics of 344 episodes. *Rev Esp Quimioter*. 2018;31(3):217–225.
16. Murray CJL, Ikuta KS, Sharara F, et al. Global burden of bacterial antimicrobial resistance in 2019: a systematic analysis. *Lancet*. 2022;399(10325):629–655. doi:10.1016/S0140-6736(21)02724-0
17. Ge J, Lei J, Zare RN. Protein–inorganic hybrid nanoflowers. *Nat Nanotechnol*. 2012;7(7):428–432. doi:10.1038/nnano.2012.80
18. Dube S, Rawtani D. Understanding intricacies of bioinspired organic-inorganic hybrid nanoflowers: a quest to achieve enhanced biomolecules immobilization for biocatalytic, biosensing and bioremediation applications. *Adv Colloid Interface Sci*. 2021;295:102484. doi:10.1016/j.cis.2021.102484
19. Le XA, Le TN, Kim M. Dual-Functional Peroxidase-Copper Phosphate Hybrid Nanoflowers for Sensitive Detection of Biological Thiols. *Int J Mol Sci*. 2021;23(1):366. doi:10.3390/ijms23010366
20. Batule BS, Park KS, Gautam S, Cheon HJ, Kim M, Park HG. Intrinsic peroxidase-like activity of sonochemically synthesized protein copper nanoflowers and its application for the sensitive detection of glucose. *Sensors Actuators B Chem*. 2019;283:749–754. doi:10.1016/j.snb.2018.12.028
21. Guo J, Wang Y, Zhao M. A self-activated nanobiocatalytic cascade system based on an enzyme-inorganic hybrid nanoflower for colorimetric and visual detection of glucose in human serum. *Sensors Actuators B Chem*. 2019;284:45–54. doi:10.1016/j.snb.2018.12.102
22. Shcharbin D, Halets-Bui I, Abashkin V, et al. Hybrid metal-organic nanoflowers and their application in biotechnology and medicine. *Colloids Surfaces B Biointerfaces*. 2019;182:110354. doi:10.1016/j.colsurfb.2019.110354
23. Liu Y, Chen J, Du M, Wang X, Ji X, He Z. The preparation of dual-functional hybrid nanoflower and its application in the ultrasensitive detection of disease-related biomarker. *Biosens Bioelectron*. 2017;92:68–73. doi:10.1016/j.bios.2017.02.004
24. Zhu J, Wen M, Wen W, et al. Recent progress in biosensors based on organic-inorganic hybrid nanoflowers. *Biosens Bioelectron*. 2018;120:175–187. doi:10.1016/j.bios.2018.08.058
25. Aydemir D, Gecili F, Özdemir N, Nuray Ulusu N. Synthesis and characterization of a triple enzyme-inorganic hybrid nanoflower (TrpE@ihNF) as a combination of three pancreatic digestive enzymes amylase, protease and lipase. *J Biosci Bioeng*. 2020;129(6):679–686. doi:10.1016/j.jbiosc.2020.01.008
26. Zhang Z, Zhang Y, Song R, et al. Manganese(II) phosphate nanoflowers as electrochemical biosensors for the high-sensitivity detection of ractopamine. *Sensors Actuators B Chem*. 2015;211:310–317. doi:10.1016/j.snb.2015.01.106
27. Zhang Z, Zhang Y, He L, et al. A feasible synthesis of Mn 3 (PO 4) 2 @BSA nanoflowers and its application as the support nanomaterial for Pt catalyst. *J Power Sources*. 2015;284:170–177. doi:10.1016/j.jpowsour.2015.03.011
28. Cui J, Jia S. Organic–inorganic hybrid nanoflowers: a novel host platform for immobilizing biomolecules. *Coord Chem Rev*. 2017;352:249–263. doi:10.1016/j.ccr.2017.09.008
29. Kim KH, Jeong JM, Lee SJ, Choi BG, Lee KG. Protein-directed assembly of cobalt phosphate hybrid nanoflowers. *J Colloid Interface Sci*. 2016;484:44–50. doi:10.1016/j.jcis.2016.08.059
30. Altinkaynak C, Tavlasoglu S, Ÿzdemir N, Ocsoy I. A new generation approach in enzyme immobilization: organic-inorganic hybrid nanoflowers with enhanced catalytic activity and stability. *Enzyme Microb Technol*. 2016;93-94:105–112. doi:10.1016/j.enzmictec.2016.06.011
31. Bilal M, Asgher M, Shah SZH, Iqbal HMN. Engineering enzyme-coupled hybrid nanoflowers: the quest for optimum performance to meet biocatalytic challenges and opportunities. *Int J Biol Macromol*. 2019;135:677–690. doi:10.1016/j.ijbiomac.2019.05.206
32. Somturk B, Yilmaz I, Altinkaynak C, Karatepe A, Özdemir N, Ocsoy I. Synthesis of urease hybrid nanoflowers and their enhanced catalytic properties. *Enzyme Microb Technol*. 2016;86:134–142. doi:10.1016/j.enzmictec.2015.09.005
33. Hao M, Fan G, Zhang Y, Xin Y, Zhang L. Preparation and characterization of copper-Brevibacterium cholesterol oxidase hybrid nanoflowers. *Int J Biol Macromol*. 2019;126:539–548. doi:10.1016/j.ijbiomac.2018.12.237
34. Gaetke LM, Chow-Johnson HS, Chow CK. Copper: toxicological relevance and mechanisms. *Arch Toxicol*. 2014;88(11):1929–1938. doi:10.1007/s00204-014-1355-y
35. Farcasanu IC, Popa CV, Ruta LL. Calcium and Cell Response to Heavy Metals: can Yeast Provide an Answer? *Calcium Signal Transduction*. 2018. doi:10.5772/intechopen.78941

36. Li K, Wang XF, Li DY, et al. The good, the bad, and the ugly of calcium supplementation: a review of calcium intake on human health. *Clin Interv Aging*. 2018;13:2443–2452. doi:10.2147/CIA.S157523
37. Giorgi C, Marchi S, Pinton P. The machineries, regulation and cellular functions of mitochondrial calcium. *Nat Rev Mol Cell Biol*. 2018;19 (11):713–730. doi:10.1038/s41580-018-0052-8
38. Wang LB, Wang YC, He R, et al. A New Nanobiocatalytic System Based on Allosteric Effect with Dramatically Enhanced Enzymatic Performance. *J Am Chem Soc*. 2013;135(4):1272–1275. doi:10.1021/ja3120136
39. Koley P, Sakurai M, Takei T, Aono M. Facile fabrication of silk protein sericin-mediated hierarchical hydroxyapatite-based bio-hybrid architectures: excellent adsorption of toxic heavy metals and hazardous dye from wastewater. *RSC Adv*. 2016;6(89):86607–86616. doi:10.1039/C6RA12818A
40. Ghosh K, Balog ERM, Sista P, et al. Temperature-dependent morphology of hybrid nanoflowers from elastin-like polypeptides. *APL Mater*. 2014;2(2):021101. doi:10.1063/1.4863235
41. Yin Y, Xiao Y, Lin G, Xiao Q, Lin Z, Cai Z. An enzyme–inorganic hybrid nanoflower based immobilized enzyme reactor with enhanced enzymatic activity. *J Mater Chem B*. 2015;3(11):2295–2300. doi:10.1039/C4TB01697A
42. Zhao F, Wang Q, Dong J, et al. Enzyme-inorganic nanoflowers/alginate microbeads: an enzyme immobilization system and its potential application. *Process Biochem*. 2017;57:87–94. doi:10.1016/j.procbio.2017.03.026
43. Liu Y, Zhang Y, Li X, Yuan Q, Liang H. Self-repairing metal–organic hybrid complexes for reinforcing immobilized chloroperoxidase reusability. *Chem Commun*. 2017;53(22):3216–3219. doi:10.1039/C6CC10319G
44. Wang X, Shi J, Li Z, et al. Facile One-Pot Preparation of Chitosan/Calcium Pyrophosphate Hybrid Microflowers. *ACS Appl Mater Interfaces*. 2014;6(16):14522–14532. doi:10.1021/am503787h
45. Ye R, Zhu C, Song Y, et al. One-pot bioinspired synthesis of all-inclusive protein–protein nanoflowers for point-of-care bioassay: detection of E. coli O157:H7 from milk. *Nanoscale*. 2016;8(45):18980–18986. doi:10.1039/C6NR06870G
46. Patel D, Haag SL, Patel JS, Ytreberg FM, Bernards MT. Paired Simulations and Experimental Investigations into the Calcium-Dependent Conformation of Albumin. *J Chem Inf Model*. 2022;62(5):1282–1293. doi:10.1021/acs.jcim.1c01104
47. Kuten Pella O, Hornyák I, Horváthy D, Fodor E, Nehrer S, Lacza Z. Albumin as a Biomaterial and Therapeutic Agent in Regenerative Medicine. *Int J Mol Sci*. 2022;23(18):10557. doi:10.3390/ijms231810557
48. Evans TW. Review article: albumin as a drug-biological effects of albumin unrelated to oncotic pressure. *Aliment Pharmacol Ther*. 2002;16:6–11. doi:10.1046/j.1365-2036.16.s5.2.x
49. Kratz F, Elsadek B. Clinical impact of serum proteins on drug delivery. *J Control Release*. 2012;161(2):429–445. doi:10.1016/j.jconrel.2011.11.028
50. Maurya P, Singh S, Mishra N, et al. Albumin-based nanomaterials in drug delivery and biomedical applications. *Biopolymer-Based Nanomaterials in Drug Delivery and Biomedical Applications*. Elsevier; 2021:465–496. doi:10.1016/B978-0-12-820874-8.00012-9
51. Kouchakzadeh H, Safavi MS, Shojaosadati SA. Efficient Delivery of Therapeutic Agents by Using Targeted Albumin Nanoparticles. *Drug Delivery Systems*. 2015:121–143. doi:10.1016/bs.apcsb.2014.11.002
52. Ipte PR, Sahoo S, Satpati AK. Spectro-electrochemistry of ciprofloxacin and probing its interaction with bovine serum albumin. *Bioelectrochemistry*. 2019;130:107330. doi:10.1016/j.bioelechem.2019.107330
53. Doble A. Ciprofloxacin. In: *XPharm: The Comprehensive Pharmacology Reference*. Elsevier; 2007:1–8. doi:10.1016/B978-008055232-3.61473-4
54. Szafran M, Zakrzewska-Czerwińska J, Jakimowicz D. Bacterial type I topoisomerases – biological function and potential use as targets for antibiotic treatments. *Postepy Hig Med Dosw*. 2013;67:130–142. doi:10.5604/17322693.1038352
55. Sharma PC, Jain A, Jain S, Pahwa R, Yar MS. Ciprofloxacin: review on developments in synthetic, analytical, and medicinal aspects. *J Enzyme Inhib Med Chem*. 2010;25(4):577–589. doi:10.3109/14756360903373350
56. Gao Y, Shang Q, Li W, et al. Antibiotics for cancer treatment: a double-edged sword. *J Cancer*. 2020;11(17):5135–5149. doi:10.7150/jca.47470
57. Kim BN, Kim ES, Oh MD. Oral antibiotic treatment of staphylococcal bone and joint infections in adults. *J Antimicrob Chemother*. 2014;69 (2):309–322. doi:10.1093/jac/dkt374
58. Paul BK, Guchhait N, Bhattacharya SC. Binding of ciprofloxacin to bovine serum albumin: photophysical and thermodynamic aspects. *J Photochem Photobiol B Biol*. 2017;172:11–19. doi:10.1016/j.jphotobiol.2017.04.026
59. Hu YJ, Ou-Yang Y, Zhang Y, Liu Y. Affinity and Specificity of Ciprofloxacin-Bovine Serum Albumin Interactions: spectroscopic Approach. *Protein J*. 2010;29(4):234–241. doi:10.1007/s10930-010-9244-6
60. Anand U, Kurup L, Mukherjee S. Deciphering the role of pH in the binding of Ciprofloxacin Hydrochloride to Bovine Serum Albumin. *Phys Chem Chem Phys*. 2012;14(12):4250. doi:10.1039/c2cp00001f
61. Verma R, Mishra SR, Gadore V, Ahmaruzzaman M. Hydroxyapatite-based composites: excellent materials for environmental remediation and biomedical applications. *Adv Colloid Interface Sci*. 2023;315:102890. doi:10.1016/j.cis.2023.102890
62. Du M, Chen J, Liu K, Xing H, Song C. Recent advances in biomedical engineering of nano-hydroxyapatite including dentistry, cancer treatment and bone repair. *Compos Part B Eng*. 2021;215:108790. doi:10.1016/j.compositesb.2021.108790
63. Mondal S, Dorozhkin SV, Pal U. Recent progress on fabrication and drug delivery applications of nanostructured hydroxyapatite. *WIREs Nanomed Nanobiotechnol*. 2018;10(4). doi:10.1002/wnan.1504
64. Varadavenkatesan T, Vinayagam R, Pai S, Kathirvel B, Pugazhendhi A, Selvaraj R. Synthesis, biological and environmental applications of hydroxyapatite and its composites with organic and inorganic coatings. *Prog Org Coatings*. 2021;151:106056. doi:10.1016/j.porgcoat.2020.106056
65. Pham HH, Luo P, Génin F, Dash AK. Synthesis and characterization of hydroxyapatite-ciprofloxacin delivery systems by precipitation and spray drying technique. *AAPS PharmSciTech*. 2002;3(1):1–9. doi:10.1208/pt030101
66. Shanaghi A, Mehrjou B, Ahmadian Z, Souri AR, Chu PK. Enhanced corrosion resistance, antibacterial properties, and biocompatibility by hierarchical hydroxyapatite/ciprofloxacin-calcium phosphate coating on nitrided NiTi alloy. *Mater Sci Eng C*. 2021;118:111524. doi:10.1016/j.msec.2020.111524
67. Anita Lett J, Sagadevan S, Fatimah I, et al. Recent advances in natural polymer-based hydroxyapatite scaffolds: properties and applications. *Eur Polym J*. 2021;148:110360. doi:10.1016/j.eurpolymj.2021.110360

68. Li N, Hu B, Wang A, et al. Facile Bioinspired Preparation of Fluorinase@Fluoridated Hydroxyapatite Nanoflowers for the Biosynthesis of 5′-Fluorodeoxy Adenosine. *Sustainability*. 2020;12(1):431. doi:10.3390/su12010431
69. Ait Said H, Noukrati H, Ben Youcef H, Mahdi I, Oudadesse H, Barroug A. In situ precipitated hydroxyapatite-chitosan composite loaded with ciprofloxacin: formulation, mechanical, in vitro antibiotic uptake, release, and antibacterial properties. *Mater Chem Phys*. 2023;294:127008. doi:10.1016/j.matchemphys.2022.127008
70. Shen B, Wen X, Korshin GV. Electrochemical oxidation of ciprofloxacin in two different processes: the electron transfer process on the anode surface and the indirect oxidation process in bulk solutions. *Environ Sci Process Impacts*. 2018;20(6):943–955. doi:10.1039/C8EM00122G
71. Trivedi P, Vasudevan D. Spectroscopic Investigation of Ciprofloxacin Speciation at the Goethite−Water Interface. *Environ Sci Technol*. 2007;41(9):3153–3158. doi:10.1021/es061921y
72. Zhao Z, Zhang J, Wang M, et al. Structure advantage and peroxidase activity enhancement of deuterohemin-peptide–inorganic hybrid flowers. *RSC Adv*. 2016;6(106):104265–104272. doi:10.1039/C6RA24192A
73. Koutsopoulos S. Synthesis and characterization of hydroxyapatite crystals: a review study on the analytical methods. *J Biomed Mater Res*. 2002;62(4):600–612. doi:10.1002/jbm.10280
74. Yadav P, Yadav AB. Preparation and characterization of BSA as a model protein loaded chitosan nanoparticles for the development of protein-/peptide-based drug delivery system. *Futur J Pharm Sci*. 2021;7(1):200. doi:10.1186/s43094-021-00345-w
75. Ozhukil Kollath V, De Geest BG, Mullens S, et al. Systematic Processing of β-Tricalcium Phosphate for Efficient Protein Loading and In Vitro Analysis of Antigen Uptake. *Adv Eng Mater*. 2013;15(4):295–301. doi:10.1002/adem.201200177
76. Kowalczuk D, Gładysz A, Pitucha M, Kamiński DM, Barańska A, Drop B. Spectroscopic Study of the Molecular Structure of the New Hybrid with a Potential Two-Way Antibacterial Effect. *Molecules*. 2021;26(5):1442. doi:10.3390/molecules26051442
77. Hussein-Al-Ali SH, Abudoleh SM, Abualassal QIA, Abudayeh Z, Aldalahmah Y, Hussein MZ. Preparation and characterisation of ciprofloxacin-loaded silver nanoparticles for drug delivery. *IET Nanobiotechnology*. 2022;16(3):92–101. doi:10.1049/nbt2.12081
78. Ozhukil Kollath V, Mullens S, Luyten J, Traina K, Cloots R. Protein–calcium phosphate nanocomposites: benchmarking protein loading via physical and chemical modifications against co-precipitation. *RSC Adv*. 2015;5(69):55625–55632. doi:10.1039/C5RA08060F
79. Füredi-Milhofer H, Hlady V, Baker FS, Beebe RA, Wikholm NW, Kittelberger J. Temperature-programmed dehydration of hydroxyapatite. *J Colloid Interface Sci*. 1979;70(1):1–9. doi:10.1016/0021-9797(79)90002-X
80. Senra MR, Lima RB, Souza D, Marques M, Monteiro SN. Thermal characterization of hydroxyapatite or carbonated hydroxyapatite hybrid composites with distinguished collagens for bone graft. *J Mater Res Technol*. 2020;9(4):7190–7200. doi:10.1016/j.jmrt.2020.04.089
81. Olivera ME, Manzo RH, Junginger HE, et al. Biowaiver Monographs for Immediate Release Solid Oral Dosage Forms: ciprofloxacin Hydrochloride. *J Pharm Sci*. 2011;100(1):22–33. doi:10.1002/jps.22259
82. Kisicki JC, Griess RS, Ott CL, et al. Multiple-dose pharmacokinetics and safety of rufloxacin in normal volunteers. *Antimicrob Agents Chemother*. 1992;36(6):1296–1301. doi:10.1128/AAC.36.6.1296
83. Lee JH, Yeo Y. Controlled drug release from pharmaceutical nanocarriers. *Chem Eng Sci*. 2015;125:75–84. doi:10.1016/j.ces.2014.08.046
84. Madni A, Tahir N, Rehman M, et al. Hybrid Nano-carriers for Potential Drug Delivery. In: *Advanced Technology for Delivering Therapeutics*. InTech; 2017. doi:10.5772/66466
85. Jin Y, Li Z, Liu H, et al. Biodegradable, multifunctional DNAzyme nanoflowers for enhanced cancer therapy. *NPG Asia Mater*. 2017;9(3):e365–e365. doi:10.1038/am.2017.34
86. Guo Y, Li S, Wang Y, Zhang S. Diagnosis–Therapy Integrative Systems Based on Magnetic RNA Nanoflowers for Co-drug Delivery and Targeted Therapy. *Anal Chem*. 2017;89(4):2267–2274. doi:10.1021/acs.analchem.6b03346
87. Nwabuife JC, Omolo CA, Govender T. Nano delivery systems to the rescue of ciprofloxacin against resistant bacteria “E. coli; P. aeruginosa; Saureus; and MRSA” and their infections. *J Control Release*. 2022;349:338–353. doi:10.1016/j.jconrel.2022.07.003
88. Ciocilteu MV, Mocanu AG, Mocanu A, et al. Hydroxyapatite-ciprofloxacin delivery system: synthesis, characterisation and antibacterial activity. *Acta Pharm*. 2018;68(2):129–144. doi:10.2478/acph-2018-0011
89. Geuli O, Metoki N, Zada T, Reches M, Eliaz N, Mandler D. Synthesis, coating, and drug-release of hydroxyapatite nanoparticles loaded with antibiotics. *J Mater Chem B*. 2017;5(38):7819–7830. doi:10.1039/C7TB02105D
90. Benedini L, Laiuppa J, Santillán G, Baldini M, Messina P. Antibacterial alginate/nano-hydroxyapatite composites for bone tissue engineering: assessment of their bioactivity, biocompatibility, and antibacterial activity. *Mater Sci Eng C*. 2020;115:111101. doi:10.1016/j.msec.2020.111101
91. Sangeetha K, Girija EK. Tailor made alginate hydrogel for local infection prophylaxis in orthopedic applications. *Mater Sci Eng C*. 2017;78:1046–1053. doi:10.1016/j.msec.2017.04.154
92. Jariya SAI, Padmanabhan VP, Kulandaivelu R, et al. Drug delivery and antimicrobial studies of chitosan-alginate based hydroxyapatite bioscaffolds formed by the Casein micelle assisted synthesis. *Mater Chem Phys*. 2021;272:125019. doi:10.1016/j.matchemphys.2021.125019
93. Leprêtre S, Chai F, Hornez JC, et al. Prolonged local antibiotics delivery from hydroxyapatite functionalised with cyclodextrin polymers. *Biomaterials*. 2009;30(30):6086–6093. doi:10.1016/j.biomaterials.2009.07.045
94. Lin L, Shao J, Ma J, et al. Development of ciprofloxacin and nano-hydroxyapatite dual-loaded polyurethane scaffolds for simultaneous treatment of bone defects and osteomyelitis. *Mater Lett*. 2019;253:86–89. doi:10.1016/j.matlet.2019.06.028
95. Choi Y, Nirmala R, Lee JY, Rahman M, Hong ST, Kim HY. Antibacterial ciprofloxacin HCl incorporated polyurethane composite nanofibers via electrospinning for biomedical applications. *Ceram Int*. 2013;39(5):4937–4944. doi:10.1016/j.ceramint.2012.11.088
96. Alinavaz S, Mahdavinia GR, Jafari H, Hazrati M, Akbari A. Hydroxyapatite (HA)-based hybrid bionanocomposite hydrogels: ciprofloxacin delivery, release kinetics and antibacterial activity. *J Mol Struct*. 2021;1225:129095. doi:10.1016/j.molstruc.2020.129095
97. Castro C, Évora C, Baro M, Soriano I, Sánchez E. Two-month ciprofloxacin implants for multibacterial bone infections. *Eur J Pharm Biopharm*. 2005;60(3):401–406. doi:10.1016/j.ejpb.2005.02.005
98. Castro C, Sánchez E, Delgado A, et al. Ciprofloxacin implants for bone infection. In vitro–in vivo characterization. *J Control Release*. 2003;93(3):341–354. doi:10.1016/j.jconrel.2003.09.004
99. Placente D, Benedini LA, Baldini M, Laiuppa JA, Santillán GE, Messina PV. Multi-drug delivery system based on lipid membrane mimetic coated nano-hydroxyapatite formulations. *Int J Pharm*. 2018;548(1):559–570. doi:10.1016/j.ijpharm.2018.07.036
100. Cao T, Tang W, Zhao J, Qin L, Lan C. A Novel Drug Delivery Carrier Based on α-eleostearic Acid Grafted Hydroxyapatite Composite. *J Bionic Eng*. 2014;11(1):125–133. doi:10.1016/S1672-6529(14)60027-5